THE EFFECT OF HERMANSON'S SPATIAL DIELECTRIC FUNCTION ON THE DENSITY OF IMPURITY STATES IN A GALLIUM ARSENIDE QUANTUM DOT (GaAs QD) OF RECTANGULAR CROSS-SECTION

LEONARD MACHUKA

A thesis submitted in partial fulfillment of the requirements for the award of the Degree of Master of Science in Physics of Pwani University

April 2018

DECLARATION

Declaration by Student

I hereby declare that this thesis is my original work and has not been presented for a degree in any other university. The secondary sources of information reviewed and used in this work are all acknowledged by means of reference.

Signature: ..... Date: 18/10/2018

Mr. Leonard Machuka (I56/PU/2038/13)

Declaration by Supervisor

This thesis has been submitted for examination with our approval as University Supervisors,

Signature: ..... Date: October 12, 2018.

Prof. H. Odhiambo Oyoko, Ph. D.,

Department of Physics, Pwani University

P.O. BOX 195 - 80108,

Kilifi – Kenya

Signature: ..... Date: 11/OCT/2018

Prof. George Odhiambo Amolo, Ph.D.,

Technical University of Kenya

P.O. BOX 52428-00200,

Nairobi – Kenya

Acknowledgment

I wish to acknowledge God, the Almighty, for giving me wisdom and knowledge to enable me undertake this work. Secondly, I wish to express my gratitude to my supervisor Professor H. Odhiambo Oyoko for welcoming me to his "THEORY DEN" where he introduced me to the Physics of Semiconductor Nanostructures and for suggesting the topic of this thesis research. Much gratitude to my lectures Professor Katana, Professor Thoruwa , Dr. Baluku and Dr. Olwendo for their sacrifice in teaching us graduate students pro bono when our class did not meet the University threshold. I also wish to thank Professor Odhiambo Amolo of University of Technical University of Kenya, for his helpful suggestions. To, Hanif, Winnie, Solo and Fred for the moments we shared together. Finally to my dear wife, Helen and our four daughters, for thank you for understanding, utmost sacrifice and encouragement.

Dedication

Prof. Jesse Machuka (late)

You laid a foundation for us in the family and inspire us beyond the grave, rest in peace knowing the good work you started continues.

Abstract

In this work, a theoretical study of the effect of Hermansons dielectric function (screening) on the density of impurity states (DOIS) of a donor impurity located in the center of a Gallium Arsenide (GaAs) Quantum Well Dot (QWD) of rectangular cross-section has been done. The density of impurity states (DOIS) of an unscreened (hydrogenic) donor impurity was calculated and compared with that of the screened (non-hydrogenic) donor impurity for the same system. The calculations were carried out using a trial wave function in the effective mass approximation. Calculations of the binding energies for the hydrogenic and non hydrogenic donor impurity as a function of the axial (growth) length of the QWD was done and the results used to compute the density of impurity states. The results show that impurity binding energies increase with decreasing quantum well axial length until about 20 nm for a constant QWD cross-section. The binding energies for the non-hydrogenic donor impurity were found to be higher than in the hydrogenic type. These results are in agreement with previous results obtained for donor impurities in quantum well wires and quantum well dots of similar geometry .The results for the density of impurity states clearly show an important feature that is a peak at lower binding energies coming from the contribution of impurities near the axial edge of the quantum well dot. It was also observed that the DOIS obtained for the non-hydrogenic donor impurities is markedly enhanced over that for purely hydrogenic donor impurities. In fact, the enhanced DOIS of the non-hydrogenic donor impurities is observed throughout the range of binding energy values considered. The findings of this research are in agreement with the results obtained by F. J. Ribeiro and A. Latge 'In their work on the density of impurity states in spherical and cubic quantum dots, the DOIS exhibited a similar trend with a sharp peak of density of states at low binding energy followed by an almost exponential decrease with increasing binding energy. In our case, we have applied a spatial dielectric function and found that it enhances the DOIS. It is therefore, important that the effect of spatial dielectric function should be considered when designing optoelectronic devices.

Table of Contents

List of Abbreviations and Acronyms

AlAs	Aluminum Arsenide
COMVD	Chemical Organic Metal Vapour Deposition
DOIS	Density of Impurity States
GaAl	Gallium Aluminum
GaAs	Gallium Arsenide
GaN	Gallium Nitride
HEMT	High Electron Mobility Transistor
InGaN	Indium Gallium Nitride
LDSS	Low Dimensional Semiconducting Systems
LPE	Liquid Phase Epitaxy
MBE	Molecular Beam Epitaxy
MOVPE	Metal Organic Vapour Phase Epitaxy
QD	Quantum Dot
QW	Quantum Well
QWW	Quantum Well Wires

List of Tables

List of Figures

INTRODUCTION

1.1 Background Information

Recent developments in fabrication techniques such as Molecular Beam Epitaxy (MBE),[1-3], Chemical metal organic vapor phase epitaxy (MOVPE) and Liquid phase Epitaxy (LPE), have made it possible for the fabrication of Low Dimensional semiconducting systems (LDSS) such as quantum wells (QW), quantum well wires (QWW), and quantum well dots (QWD)[3,4]. The study of such low dimensional semiconducting systems (LDSS) is a major branch of what is nowadays called nanophysics. Recent major innovations in the field of electronic and optical device applications have emerged from such systems. These include electronic equipment and gadgets found in our homes such as flat screen televisions, mobile phones, and machines in hospitals and industries.

Studies in LDSS have thus attracted intense interest because of the key roles QW, QWW and QWD are playing in many of the scientific and technological innovations that have dramatically changed our lifestyle. The study of impurities states in these nanostructures is thus one of great significance. One of the most widely used semiconductor material for fabricating nano devices is Gallium arsenide ($GaAs$), usually, embedded in Gallium aluminum arsenide ($Ga_x Al_{1-x} As$).In our study, we have calculated the effect of Hermanson's spatial dielectric function on the density of impurity states (DOIS)of a $GaAs$ Quantum well dot of rectangular cross-section. We first calculated donor impurity binding energies and from these we derived the DOIS for the hydrogenic and non-

hydrogenic donor impurity. We have used the dielectric function suggested by Hermansons which has the form,

$$\frac{1}{\varepsilon(x,y,z)} = \frac{1}{\varepsilon_0} + \left\{ 1 - \frac{1}{\varepsilon_0} e^{-\left(\frac{x^2+y^2+z^2}{c}\right)^{\frac{1}{3}}} \right\} \tag{1.1}$$

Where, c is a lattice constant. The value of c which is used in this current work is $c = 0.8 a.u^{-1}$ which was obtained by Csavinzky and Oyoko [5]. The confining potential in this case is a function of this spatial dielectric function; hence the binding energy of the donor impurity in turn depends on the spatial dielectric function.

1.2 Gallium Arsenide

Gallium arsenide has some electronic properties which make it superior over silicon. Like other compound semiconductors, *GaAs* has a higher electron mobility hence allow for operation in the microwave range (1 – 1000 GHz). The hetero-junction nature also increases the gain and efficiency of amplifiers made from these devices. *GaAs* devices are relatively insensitive to overheating owing to their wider energy band gap [6]. They also tend to create less noise in electronic circuits than silicon devices, especially at high frequencies [7]. These superior properties are compelling reasons why *GaAs* circuitry is used in mobile phones, satellite communications, microwave point-to-point links and higher frequency radar systems [8].Another advantage of *GaAs* is that it has a direct band gap, which means that it can be used to absorb and emit light efficiently. Silicon has an indirect bandgap and so is relatively poor at emitting light. As a wide direct band gap material, it has a high resistance to radiation damage; this makes it an excellent material for outer space electronics, optical windows in high power applications and lasers [9].

The high resistance to radiation damage, combined with its high dielectric constant, makes *GaAs* a very good nano material used in electronic and optical devices. For example, it is an ideal material for Fabrication of microwave and millimeter wave integrated circuits (MMIC), where active and essential passive components can readily be produced on a single slice of *GaAs* [10]. Complex layered structures of gallium arsenide in combination with aluminum arsenide (AlAs) or the alloy can be grown using molecular beam epitaxy (MBE) or metal organic vapor phase epitaxy (MOVPE). *GaAs* and AlAs have nearly matched lattices that are desired to minimize defects and increase electron mobility. This produces extremely high performance and high electron mobility transistor (HEMT) and other quantum well devices [11].

1.3 Quantum Dot

When one or more of the dimensions of a solid are reduced sufficiently, its physicochemical characteristics notably depart from those of the bulk solid. With the reduction in size, novel electrical, mechanical, chemical, magnetic, and optical properties appear. The resulting structure is then called a low-dimensional structure or nanostructure. Our interest is in zero-dimensional (0-D) structure or quantum dots in which quantization occurs in all three spatial directions. The electronic and optical properties of quantum dots are closely related to the size and geometrical shape of the individual crystals [12].The main advantage of quantum dots over other heterostructures is foremost the ability to control the geometry of the quantum dots for many applications. Secondly the sensitive dependence of their electronic and optical properties on dopants provides an extensive range of tunable phenomena which can be used in devices applications. Owing to their nano-size, they have very sharp density of states

and thus excellent transport and optical properties for detectors, lasers and amplifiers [4, 7, 11].

GaAs quantum dots are fabricated using Liquid-Phase Epitaxy (LPE) or Molecular Beam Epitaxy (MBE) techniques. These techniques are well suited for the preparation of a wide range of compound semiconductor nanostructures as stoichiometric adjustments to allow control of the band structures and lattice constants. This affects both the electrical, thermal and optical properties and the epitaxial nature of the film. LPE method, involves the precipitation of a crystalline film from a supersaturated melt of *GaAs* on to a *GaAl* substrate. The *GaAs* melt is heated until phase transition occurs before the temperature is reduced for precipitation. By controlling cooling rates the kinetics of layer, growth can be manipulated. The advantages of LPE over other growth techniques are substantial, primarily in material purity, doping flexibility, and dimensional control. It has particular advantages too, in achieving the complex multilayer structures required for many interesting optical devices, such as injection lasers, light emitting diodes, and photodetectors [6].It is also a low cost technique which yields nanostructures of controlled composition, thickness and lower dislocation densities. However, LPE has the disadvantages of producing a rough surfaces and poor thickness uniformity. Molecular beam epitaxy (MBE) solves that issue [13].

1.4 Confinement and Bandgap

The reduction in dimensions of semiconductor materials increases the binding energy of donor impurities which are introduced into such materials. In the zero dimensional structure such as *GaAs / AlAs* quantum dot, the difference between the band gaps in the

two semiconductors effectively confines a free donor in the $GaAs$ layer. This is because the electron at top of the $GaAs$ conduction band does not have enough energy to reach the conduction band of $Ga_{1-x}Al_xAs$ (See Figure 1.1).

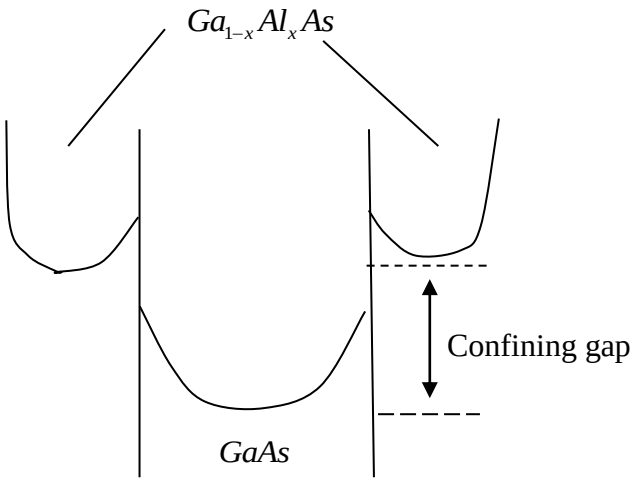

Figure 1.1: Electron confinements in GaAs/Ga1-xAlxAs heterostructure device showing the confining gap between GaAs and two Ga1-xAlxAs layers.

When the size of the QDs is decreased, the energy states will become discrete reducing the energy gap. Increased confinement in quantum dots will also increase the energy level spacing of the system. QDs are bandgap tunable by size hence their optical and electrical properties can be engineered to meet specific applications, a phenomenon related to optical and electronic properties of the material. The DOIS depends on the number of confined levels [14].

1.5 Significance of the Research Study

Low dimensional semiconductor nano-structures such as quantum wells, wires and dots have gained great importance in recent days due to their fundamental properties and their wide range of applications. A great amount of experimental and theoretical work has been devoted to the quantitative study of the physical properties of donor impurities in $GaAs/\ Ga_{1-x}Al_xAs$ (QWs), quantum-well wires (QWWs) and quantum dots (QDs) [15–19]. An understanding of the effects of impurities on the electronic and optical properties is of fundamental importance in semiconductor physics. Therefore, our study of the effect of Hermanson's spatial dielectric functions on the density of impurity states of $GaAs/Ga_{1-x}Al_xAs$ quantum well dot is one of great significance.

1.6 Research Objective

1.6.1 Main Objective

The main objective in this study was to theoretically study the effects of Hermanson's spatial dielectric function on the density of impurity states in a Gallium arsenide quantum dot of rectangular dimensions.

1.6.2 Specific Objectives of the Study

The specific activities in this study include to:

1. Set up the Hamiltonian for the hydrogenic and non-hydrogenic impurity.
2. Construct the appropriate trial wave function for the donor impurity.
3. Compute binding energy for both hydrogenic and the non-hydrogenic donor impurities.

4. Compute the density of impurity states for the hydrogenic and non-hydrogenic donor impurities.

LITERATURE REVIEW

2.1 Introduction

The physics of shallow-donor impurity states in semiconductor quantum-dot structures is an interesting area of research owing to their electronic and optical properties. QD are zero dimensional structures with ultimate quantum confinement effects where electrons are confined in all three dimensions. In recent past, increasing attention has been focused on zero-dimensional nanometer-sized Structures which can be used in device applications for example lasers as single photon optics for quantum computing and light emitting diodes. In this chapter, we have looked at previous research works that are relevant and related to this research study.

2.2 Related Research Studies in Low Dimensional Structure Systems

S. Dalgic*et al*[20] have used a variational technique to calculate the effect of an electric field on the non-hydrogenic binding energy of a donor impurity in a square $GaAs/Ga_{1-x}Al_xAs$ quantum well wire (QWW). The results showed that the non-hydrogenic binding energy of the donor impurity located around the centre is larger than that of the hydrogenic binding energy. They also showed that the donor binding energy depends sensitively both on the external electric field and the position of the quantum well walls. In both cases, the binding energy increased as the electron pushed towards the coulomb centre. Oyoko [21] studied the effect of Hermansons spatial dielectric function on the impurity binding energy in a cylindrical cross-sectional $GaAs/Ga_{1-x}Al_xAs$ QWW under zero electric field. He concluded that the effect of the spatial dielectric function

increased the binding energy of the non-hydrogenic donor impurity with decreasing radius over that of a hydrogenic donor impurity.

Pan Jiang-Hong, Liu Li-Zhe, and Liu [22-24] have investigated the influence of applied electric field on a shallow donor in $GaAs/Al_xGa_{1-x}As$ QD with variational methods. They have shown that the binding energy of this system is dependent on the complex interplay of spatial confinement, coulomb interaction and the electric field confinement. With decreasing QD size, the electronic wave function will begin to penetrate the surrounding potential barrier and then lead to a maximum binding energy occurrence.

C. A Duque *et al* [25] have calculated the density of impurity states (DOIS) for a homogeneous distribution of acceptor impurities within the low-dimensional heterostructure. They have reported that for dimensions of the system in which the length is much larger than the radius we obtain two well-defined peaks, associated with acceptors either at the on-centre position or at the edge position in the low-dimensional system. A similar study by Oyoko [26] on the effect of stress on the density of shallow donor impurities in a GaAs quantum well has also shown a variation of DOIS with binding energy having two peaks. Increased stress delays the onset of variation of DOIS with donor impurity binding energy. Khordada [27] has investigated the effect of position-dependent effective mass on the binding energy for the hydrogenic donor impurity in a cubic quantum dot. His investigations show that the binding energy decreases as the dot length increases in both the cases of constant and variable masses.

F. J. Ribeiro and A. Latge' [28] have calculated the ground-state impurity binding energy and density of impurity states in a cubic *GaAs* QD with emphasis placed on comparisons between results of the impurity binding energy of donors in cubic and spherical QD's. Their findings show that the impurity binding energies of on-center donors in spherical and cubic quantum dots are very similar provided the structures have the same volume. Their calculation for the spherical and cuboid geometry reveal that in both cases, the impurity density of states have the same important feature that is a peak at lower energies coming from the contribution of impurities near the edge of the small systems, which seems to be a signature of the quasi zero-dimensional system. The shapes of the density of states do not depend on the geometric details of the quantum systems but rather depends on the volume. To the best of our knowledge there are no theoretical studies carried out on the effects of Hermanson's spatial dielectric function on the density of impurity states of a hydrogenic and non hydrogenic -donor impurity in a QD of rectangular geometry. The findings of this study will hence enrich our understanding of the electronic and optical properties of low-dimensional semiconductor systems for device applications.

THEORY

3.1 Band structure of a Semiconductor

Semiconductors are materials with two bands separated by an energy gap. The lowest band is called the valence band and the upper band is called the conduction band. The two bands are separated by an energy gap. At temperature, T = 0 K, all the states of the valence band are occupied and the conduction band is empty. The material is thus a perfect insulator. The true energy gap is small enough to make an excitation of an electron from the valence band to the conduction band possible. At 0K, the valence band is completely full whereas the conduction band is completely empty. At T > 0 K, electrons in the valance band are thermally excited into the conduction band and contribute to the electrical conductivity; hole conduction in the valence band and electron conduction in the conduction band.

3.2 Impurity States

When dopants are added to a semiconductor, its electrical properties are altered. This process is called doping. Impurities are purposely introducing into an intrinsic semiconductor in a controlled manner in order for it to have certain desired electrical properties. Such impurities “create” energy levels in the band gap, close to conduction band edge. When the impurity has one electron more than the semiconductor, the extra electron from a donor can be treated as a positive charge with a single electron within its Coulomb potential. Such impurities are called “hydrogenic donors”. The energy levels created are “shallow” levels because of their closeness to the conduction band edge. This makes it easier to ionize the “atom” as the energy required will be small (see Figure 3.1)

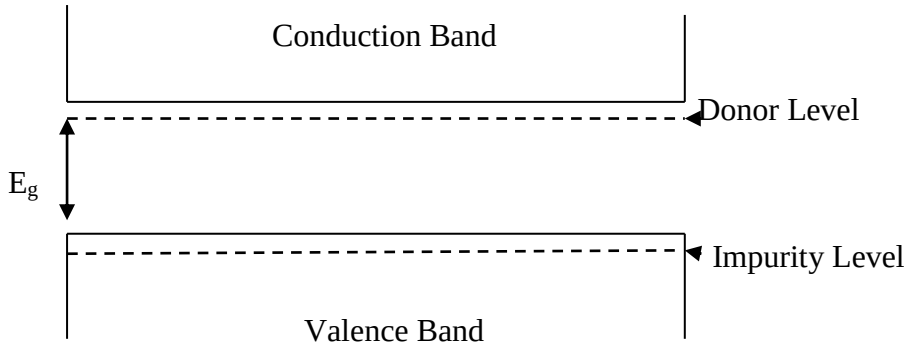

Figure 3.1: The band gap structure with Donor and acceptor levels of a semiconductor. Notice the donor and acceptor levels are close to the band edge of the conduction band and valence band respectively

When the impurity has one electron less than the semiconductor, energy levels within the band gap are created close to the valence band. This is so that the energy required to ionize the atom (accept the electron that fills the hole and creates another hole further from the substituted atom) is small. These are similar to "negative" hydrogen atoms thus referred to as hydrogenic acceptor impurities**.** The free electron is attracted back to this positive charge and forms a bound state that is just like a hydrogen atom. Their main difference between a real hydrogen atom and this bound state of an electron in the conduction band and the impurity nucleus is that the electron has effective mass, m_e which is very different from the mass of the actual electron (and is typically smaller than the bare mass of the electron).

3.3 The Number and Density of Quantum States

Optoelectronic and other transport properties significantly depend on the energy states of electrons. It is therefore important to consider the number of available states in a

certain energy range in a given band. This is known as the density of states and is denoted by a function g(E).The density of states, defines the number of quantum states, N, corresponding to the unit energy interval in the vicinity of E. In a zero-dimensional system, the electron motion is restricted in all three directions; the electron energy spectrum becomes totally discrete as in an isolated atom.

3.4 Optical Effects of Impurities in Semiconductors

The interaction of light with semiconductors gives an important and powerful technique for investigating their properties. The presence of impurities in a material will affect its optical properties and also alter its electrical conductivity. This will obviously affect the way the material interacts with light. The introduction of new energy levels within the gap brings about new optical transitions between impurity states from the bands to the new impurity states. Before the introduction of impurities, the lowest energy transition that can be made is the full band gap energy.

3.5 Numerical Computation

In this work, we have used the variational technique in the effective mass approximation to compute the density of impurity states in a quantum dot of rectangular dimensions. The success of this method relies on the trial wave function and the motivation is that the problem is recast into a more suitable form that is solvable numerically. Our starting point was the three-dimensional Hamiltonian as depicted in equations (3.1) and (3.2) for hydrogenic and non-hydrogenic case respectively.

$$H = \frac{-\hbar^2}{2m^*}\left[\frac{\partial^2}{\partial x^2}+\frac{\partial^2}{\partial y^2}+\frac{\partial^2}{\partial z^2}\right]-\frac{e^2}{4\pi\varepsilon_o}\frac{1}{\left(x^2+y^2+z^2\right)^{\frac{1}{2}}}+V_B\left(x,y,z\right) \qquad (3.1)$$

$$H = \frac{-\hbar^2}{2m^*}\left[\frac{\partial^2}{\partial x^2}+\frac{\partial^2}{\partial y^2}+\frac{\partial^2}{\partial z^2}\right]-\frac{e^2}{4\pi\varepsilon(x,y,z)}\frac{1}{\left(x^2+y^2+z^2\right)^{\frac{1}{2}}}+V_B(x,y,z) \tag{3.2}$$

Where;

$m^* = 0.067m_e$, is the effective mass of an electron.

V_B is the confining potential given by;

$$V_B(x,y,z) = \begin{cases} 0 & |x| \le \frac{L_x}{2}, |x| \le \frac{L_y}{2}, |x| \le \frac{L_z}{2} \\ \infty & otherwise \end{cases} \tag{3.3}$$

and, $\varepsilon(x,y,z)$ Is the spatial dielectric screening function given in equation (1.1), whose graphical form is shown in Figure 3.1.

Where $r = \sqrt{x^2+y^2+z^2}$

We have used a trial wave function, which is a modified by an additional term that represents the hydrogenic impurity as given in equation (3.4).

$$\psi(x,y,z) = N\cos\alpha x\cos\beta y\cos\lambda z e^{-\delta\sqrt{(x^2+y^2+z^2)}} \tag{3.4}$$

Where N is the normalization constant and δ is the variational parameter. $\alpha, \beta, and \lambda$ are constants. The cosine functions confine the donor impurity inside the QWD.

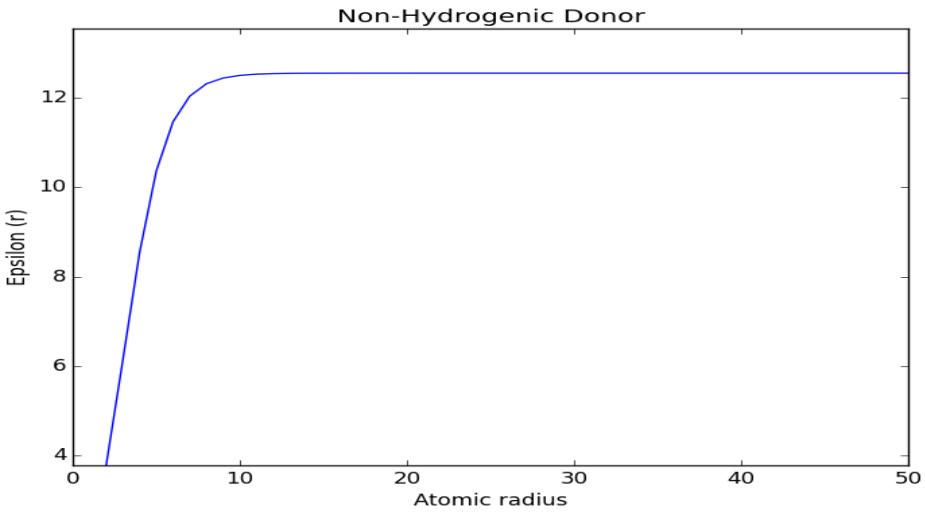

Figure 3.2: The variation of spatial dielectric function with dot size. The spatial dielectric function approaches the constant dielectric function εo for a large quantum dot size [21]

The total energy $\langle H \rangle$ for the hydrogenic donor impurity is computed using the Hamiltonian in equation (3.1) and the trial wave function, equation (3.4).

$$\langle H \rangle = \frac{\langle \psi_{1s} | H | \psi_{1s} \rangle}{\langle \psi_{1s} | \psi_{1s} \rangle} \tag{3.5}$$

The kinetic energy $\langle T \rangle$ is calculated using equation (3.6)

$$\langle \hat{T} \rangle = \frac{\hbar^2 N^2}{2m^*}\left\{\alpha^2+\beta^2+\lambda^2-\delta^2\right\}\int_0^{l_x}\cos^2\alpha x dx\int_0^{L_y}\cos^2\beta y dy\int_0^{\frac{L_z}{2}}\cos^2\lambda z\exp\{-2\delta[x^2+y^2+(z)^2]^{\frac{1}{2}}dz$$

$$+\frac{2\hbar^2 N^2\delta}{2m^*}\int_0^{l_x}\cos^2\alpha x dx\int_0^{L_y}\cos^2\beta y dy\int_0^{\frac{L_z}{2}}\frac{\cos^2\lambda z\exp\{-2\delta[x^2+y^2+(z)^2]^{\frac{1}{2}}\}dz}{\left[x^2+y^2+(z)^2\right]^{\frac{1}{2}}}$$

$$-\frac{2\hbar^2N^2\alpha\delta}{2m^*}\int_0^{L_x} x\cos\alpha x\sin\alpha x dx\int_0^{L_y}\cos^2\beta y dy\int_0^{\frac{L_z}{2}}\frac{\cos^2\lambda z\exp\{-2\delta[x^2+y^2+(z)^2]^{\frac{1}{2}}\}}{\left[x^2+y^2+(z)^2\right]^{\frac{1}{2}}}dz$$

$$\frac{2\hbar^2N^2\beta\delta}{2m^*}\int_0^{L_x}\cos^2\alpha x dx\int_0^{L_y} y\cos\beta y\sin\beta y dy\int_0^{\frac{L_z}{2}}\frac{\cos^2\lambda z\exp\{-2\delta[x^2+y^2+(z)^2]^{\frac{1}{2}}\}}{\left[x^2+y^2+(z)^2\right]^{\frac{1}{2}}}dz$$

$$-\frac{2\hbar^2N^2\lambda\delta}{2m^*}\int_0^{L_x}\cos^2\alpha x dx\int_0^{L_y}\cos^2\beta y dy\int_0^{\frac{L_z}{2}}\frac{(z)\sin\lambda z\cos\lambda z\exp\{-2\delta[x^2+y^2+(z)^2]^{\frac{1}{2}}\}}{\left[x^2+y^2+(z)^2\right]^{\frac{1}{2}}}dz$$

(3.6)

The potential energy $\langle V\rangle$ is given by;

$$\langle V\rangle=\frac{-e^2N^2}{4\pi\varepsilon_o}\int_0^{L_x}\cos^2\alpha x\,dx\int_0^{L_y}\cos^2\beta y dy\int_0^{\frac{L_z}{2}}\frac{\cos^2\lambda z\exp\{-2\delta[x^2+y^2+(z)^2]^{\frac{1}{2}}\}}{\left[x^2+y^2+(z)^2\right]^{\frac{1}{2}}}dz \quad (3.7)$$

WhereN^2 is the square of the normalization constant and is given by;

$$N^2=\left[\int_0^{\frac{L_x}{2}}\cos^2(\alpha x)dx\int_0^{\frac{L_y}{2}}\cos^2(\beta y)dy\int_0^{\frac{L_z}{2}}\cos^2(\lambda z)dz\right]^{\frac{1}{2}} \quad (3.8)$$

The details of the calculation for kinetic and potential energy are given in appendix A.

The total energy $\langle H\rangle$ for the non-hydrogenic donor is computed in equations (3.6) and (3.7).

For this case, the dielectric constant was replaced with a spatial dielectric function $\varepsilon_0 = \varepsilon(x, y, z)$

$$\frac{1}{\varepsilon(x,y,z)} = \frac{1}{\varepsilon_0} + \left\{ 1 - \frac{1}{\varepsilon_0} e^{-\left(\frac{x^2+y^2+z^2}{c}\right)^{\frac{1}{3}}} \right\} \tag{3.9}$$

The additional term which is brackets in equation (3.9) was treated separately as a small quantity in the expectation value of the total energy as given by equation (3.10).

$$\langle E \rangle_{nh} = \langle H \rangle + \Delta U \tag{3.10}$$

The total energy $\langle H \rangle$ is then minimized with respect to the variational parameter subject to the condition in equation (3.11).

$$\frac{\partial < H >}{\partial \delta} = 0 \tag{3.11}$$

This computation gave us the lowest energy; which according to the variational principle is the closest to the energy of the true state of the system (which is the equilibrium state). The value of δ obtained from equation (3.11) is plugged back into equation (3.6) which is then integrated term by term numerically and the results added to obtain the minimum total energy, $\langle \mathrm{E} \rangle_{\min}$.

The binding energy was then obtained by subtracting the minimum energy from that of the free particle energy, as given in equation (3.12).

$$E_b = \langle E \rangle_{free} - \langle E \rangle_{\min} \tag{3.12}$$

Details of the calculation of free energy are shown in appendix B.

The binding energy was then used to compute the density of impurity states for the hydrogenic and non-hydrogenic donor type using equation (3.13).

$$g\left(E_b\right)=\frac{1}{L_x L_y L_z}\int\frac{\nabla L}{\left|\nabla(E_b)\right|} \tag{3.13}$$

A detailed python code that was used to in all numerical computations is given in appendix C.

RESULTS AND DISCUSSIONS

4.1 Binding Energy as a Function of Quantum Well Dot Size for the Hydrogenic Donor

The results of the present calculations for variation of binding energy with the size of the quantum dot for the hydrogenic donor are shown in table 4.1(appendix D). The same results are shown in Figure 4.1.

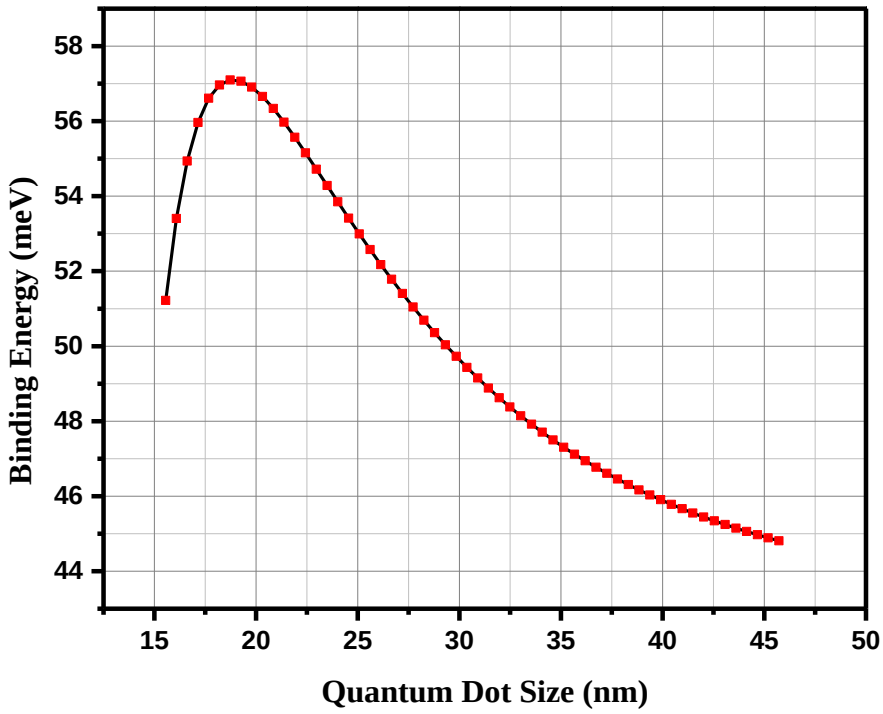

Figure 4.1: Binding energy as a function of Dot size for the non- hydrogenic donor impurity. The binding energy rises fast to a peak value of 57 meV with increase in dot size then decreases as the dot size is increased.

From the graph, we observe that the binding energy increases with decreases of dot size reaching a peak value of 57 meV at about 18nm. When the size of the dot is further

reduced, the binding energy then decreases faster than it rose. This is because as the dot width decreases both the Coulomb interaction and the tunneling effect increase. The former increases the binding energy while the latter decreases it. At about L= 18nm, some kind of equilibrium is reached between the two mechanisms leading to a maximum in the binding energy.

The results for the variation of Binding energy as a function of Dot size for the non-hydrogenic donor impurity are shown in Figure 4.2.The plot shows a similar trend as in the case with a constant dielectric function except that the binding energy peaks at 57.26 meV which is higher than the value for hydrogenic donor of similar geometry by about 0.20meV.This increase is due to the screening effect of the spatial dielectric function.

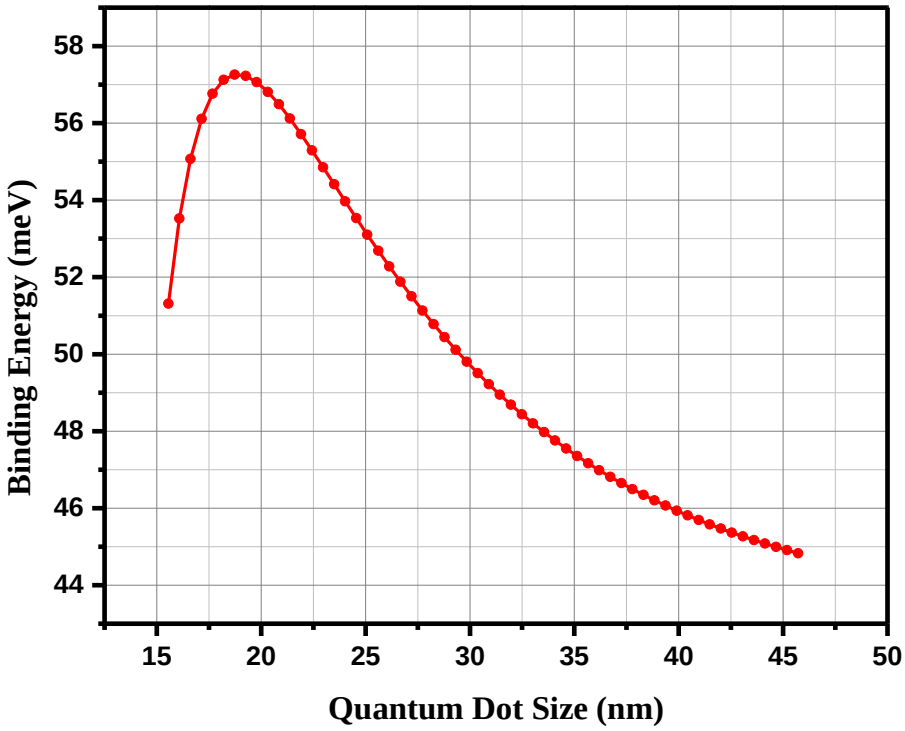

Figure 4.2: Binding energy as a function of Dot size for the non- hydrogenic donor impurity. The results show a similar trend as in the case with a constant dielectric function except that the binding energy peaks at 57.26 meV which is higher than the value for hydrogenic donor of similar geometry by about 0.20meV.This is due to the screening effect.

Figure 4.3 shows the two graphs for comparison of binding energies for donor impurities in the hydrogenic and non-hydrogenic regime.

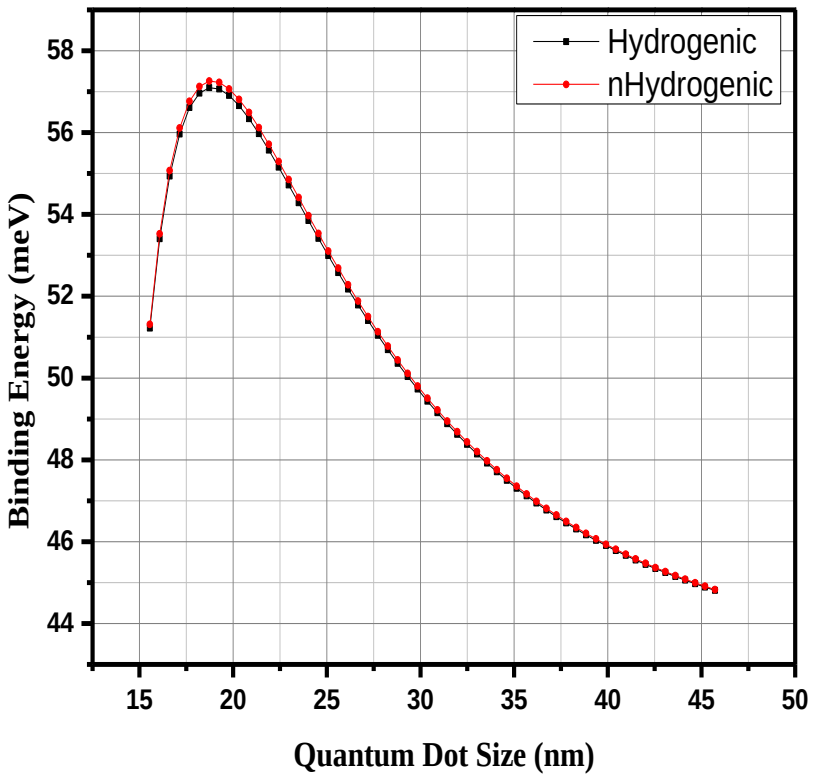

Figure 4.3: Binding energy as a function of Dot size for the hydrogenic and non-hydrogenic donor impurity. The binding energy sharply rises to a peak with increase in dot size then decreases almost exponentially with increase in axial length.

From the graphs, we observe that the values of binding energy for the non-hydrogenic donor are slightly higher due to the screening effect especially at small lengths. There is however no significant difference in binding energies at quantum sizes above 30nm.This is because quantum size effect reduces and the binding energy tends to the bulk value. The effect of Hermansons spatial dielectric function is that it increases the binding energy of the non-hydrogenic impurity with decreasing size of the quantum dot faster than in the hydrogenic type.

4.2 Effects of Binding Energy on Density of Impurity States in Ground State.

Figure 4.4 show the results of how density of impurity states varies with binding energy for the hydrogenic donor.

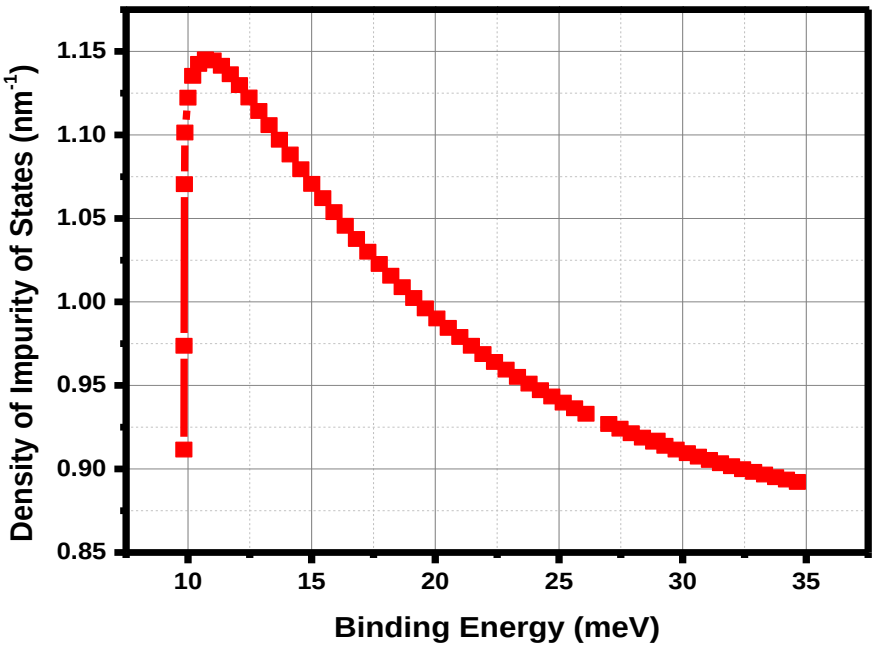

Figure 4.4: Density impurity states as a function of binding energy for the hydrogenic donor. The DOIS quickly rises to a peak value and then decreases with increase in binding energy

From Figure 4.4, we observe that the density of impurity states starts at about 0.92 /nm and sharply increases to a peak of 1.15/nm at about 10.7meV. There is then a sharp and almost exponential drop in DOIS to a value of about 0.87/nm at about 35 meV. The differences in DOIS significantly show up below 25 meV and show more deviations as the binding energy decreases up to about the peak value.

Figure 4.5 shows the results for variation of the density of impurity states with the binding energy for the non-hydrogenic donor.

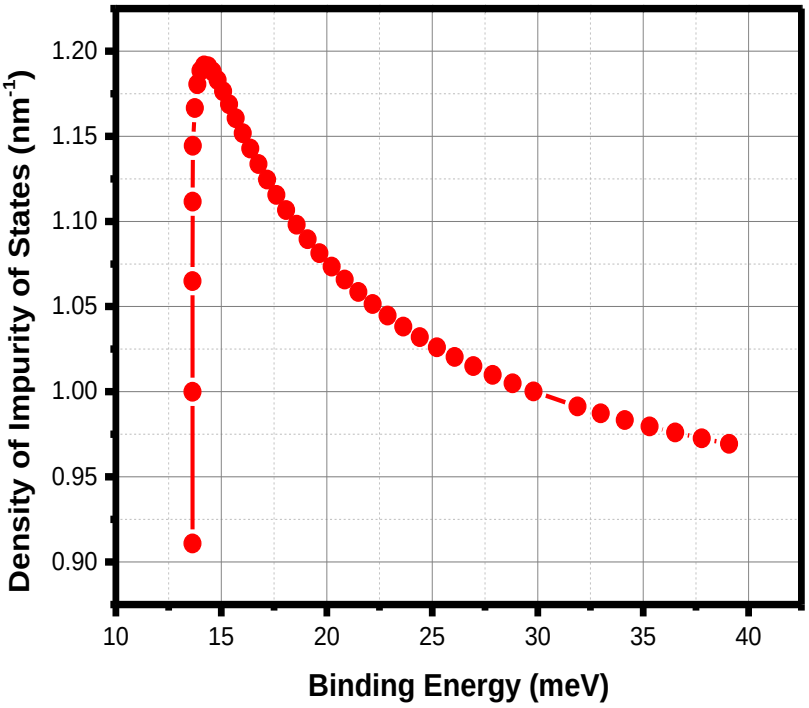

Figure 4.5: Density of impurity states as a function of binding energy for a non-hydrogenic donor impurity. Notice the DOIS sharply rises to a peak and then decreases almost exponentially with increase in binding energy

From the graph, we notice a similar trend as in the case of the hydrogenic donor impurity. The onset of DOIS is about 0.92 /nm rising sharply to a peak of about 1.19/nm at about 13.5 meV. The DOIS then reduces almost exponentially to about 0.90/nm at about 38 meV. The results for the density of impurity states for both cases clearly show an important feature that is a peak at lower binding energies, which is the defining feature for 0-D structures. This is as a result of the contribution of impurities near the

axial edge of the quantum well dot. This effect becomes more and more pronounced as the dimensionality of the active layer is reduced making injected charge carriers concentrate in an increasingly narrower energy range near the band edge.

Figure 4.6, is a graph of the DOIS as a function of the binding energy for both hydrogenic and non-hydrogenic donor impurities.

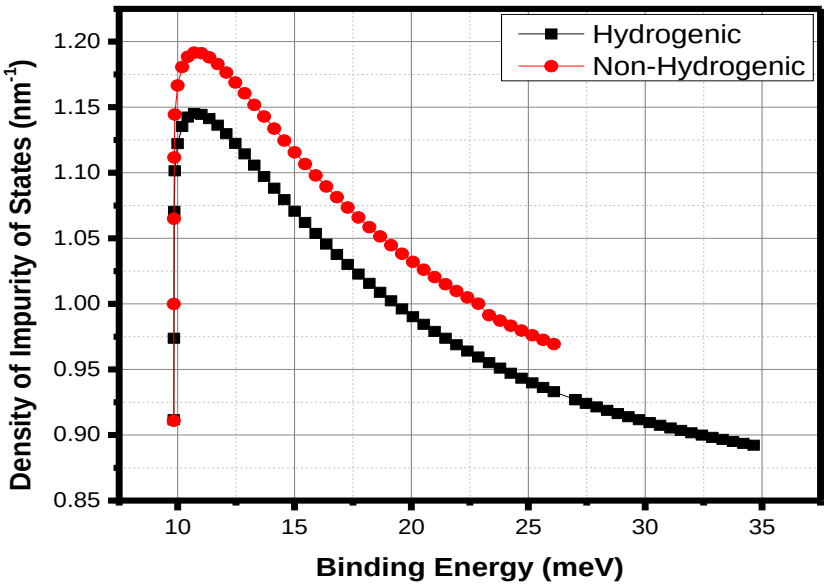

Figure 4.6: A comparison of the density of impurity states as a function of binding energy for both hydrogenic and non-hydrogenic donors. The DOIS for the non-hydrogenic donor is higher than that for the hydrogenic donor.

From the plots, we observe that DOIS for non-hydrogenic donor impurities is higher than that for the hydrogenic donor right from the onset of DOIS through their peaks and in fact the former becomes larger as the binding energy increases. This is reasonable because as the donor impurity approaches the donor ion core, it is less screened by the dielectric function since the dielectric function approaches the dielectric constant while

the donor moves further away from the parent ion, the screening becomes more pronounced.

CONCLUSION AND RECOMMENDATION

5.1 Conclusion

We have performed a theoretical calculation related to the effect of Hermansons spatial dielectric function on the density of impurity states (DOIS) in $GaAs/Ga_{1}\text{-}xAl_{x}\,As$ QD of rectangular cross-section using a variational procedure within the effective mass approximation. The important findings of this research are that;

1 The donor binding energy increases when the quantum dot size decreases reaching a peak value at a particular length, then decreases when the length reduces further.

2 Binding energies for the non hydrogenic donor impurity were found to be slightly above those for the hydrogenic donor impurity for the same dot size,

3 The density of impurity states DOIS starts at a particular value and sharply increases to a peak at low binding energy. This is then followed by a sharp and almost exponential drop in DOIS to an almost flat value at higher binding energy.

4 The DOIS for the non-hydrogenic donor impurity was much larger than that of the hydrogenic donor impurity throughout the range of binding energies considered

5 The effect of the dielectric function (screening) is that it enhances the DOIS above in the non-hydrogenic donor impurity over the hydrogenic (unscreened) donor impurities.

We hope that the findings of this research will add to knowledge and understanding of experimental results related to optical phenomena associated with shallow donor impurities in quantum well dots of different geometry.

5.2 Recommendations

In order to enhance better understanding of transport phenomena in 0D systems, it is recommended that further investigations be undertaken to determine the effect of the spatial dielectric function on density of impurity states for quantum dots made from semiconductor materials with more elegant properties such as Gallium Nitride (GaN) or Indium Gallium Nitride (InGaN).

REFERENCES

1. E.H.C Parker, Technology and physics for molecular beam Epitaxy (Plenum press, New York (1985)
2. Dewey G.; Hudait, Mantu, K.; Kangho, L.; Pillarisetty, R.; Rachmady, W.; Radosavljevic, M.; Rakshit, T.;Chau, R. *I.E.E.E. Electron Device Letters* 2008, 29,1094
3. Fujihashi, C.; Yukiya, T.; Asenor, A. *I.E.E.E. Trans. on Nano Technology* 2007, 6, 320.
4. Quarg, D.N.; Tung, N. H.Band bending effects on the electronic properties of square quantum well ,*Phys. Rev. B* 2008, 77, 125335.
5. P. Martyniuk and A. Rogalski, "Quantum-Dot Infrared Photodetectors: Status and Outlook," Progress in Quantum - Electronics, Vol. 32, No. 3-4, 2008, pp. 89-120
6. Csavinszky and Oyoko. Binding energy of on-axis hydrogenic and non-hydrogenic donors in a GaAs/$Ga_{1-x}Al_xS$ quantum well wire of circular cross section. Phys. Rev. B 43, 9262 – Published 15 April 1991
7. P. Martyniuk and A. Rogalski, "Quantum-Dot Infrared Photodetectors: Status and Outlook," Progress in Quantum Electronics, Vol. 32, No. 3-4, 2008, pp. 89-120.
8. A. A. Lagatsky, et al "Ultra short-Pulse Lasers Passively Mode Locked by Quantum-Dot-Based Saturable Absorbers," Progress in Quantum Electronics, Vol. 34, No. 1, 2010, pp. 1-45.J.
9. Harbold and M. Plisch, "The Quantum Dot," Cornell University, 2008.
10. Kooyong, S.; Soak, K.J.; Key, K.E.; Mei, H.S. *Nanotechnology 2010, 21,* 134026.
11. Milton Ohring, Reliability and failure of electronic materials and devices. Academic press,1998, ISBN 0-12-524985-3,p310.

12. John Dakin, Robert G. W. Brown, Handbook of optoelectronics volume 1, CRC press,2006 ISBN 0-7503-0646-7 P.57
13. Ephrem O. Chukwuocha et al, Theoretical Studies on the Effect of Confinement on Quantum Dots Using the Brus Equation, World Journal of Condensed Matter Physics Vol.2 No.2(2012),
14. Compound semiconductors and Crystal Growth Techniques Fundamentals of Solid State Engineering pp 349-386
15. Harrison, *Quantum Wells, Wires and Dots: Theoretical and Computational Physics* ~Wiley, Chichester, (1999)
16. N. Porras-Montenegro, S.T. Perez-Merchancano, Binding energies and density of impurity states in spherical GaAs-(Ga,Al)As quantum dot .*J Appl Phys* **74** (1993) 7624.
17. J. Silva-Valencia and N Porass Montenegro Optical absorption spectra associated with shallow donor impurities in spherical infinite-well GaAs quantum dots .*J. Appl. Phys.* **81** (1997) 901
18. H.O. Oyoko, C.A. Duque, and N. Porras-Montenegro, Uniaxial stress dependence of the binding energy of shallow donor impurities in GaAs(Ga,Al)AS quantum dots.*J. Appl. Phys.* **90** (2001) 819-823.
19. Shreemant Raman LK Mishra, Binding energy evaluation of a nano dot as a function of Dot radius at different concentrations. J. of pure appl. and ind. Phys.vol 3(4)257-263 (2013)
20. S. Dalgic, M. Ula, B. Ozkapi , Electric field effect on the binding energy of a non-hydrogenic donor impurity in a square quantum well wire; journal of Optoelectronics and Advanced Materials Vol. 7, No. 4, August 2005, p. 2041 – 2046

21. H. Odhiambo Oyoko, Effect of Hermanson's spatial dielectric function on the donor impurity binding energy in a cylindrical cross section GaAs/GaAlAs quantum well wire if infinite length. Ind. J. of Pure& Appl. Phys. **38**, 512 (2000)
22. Pan, J. H., Liu, L. Z., & Liu, M. (2011). Hydrogenic-donor impurity states in GaAs/Al x Ga 1− x As quantum dots in the presence of an electric field. *Chinese Physics Letters*, *28*(8), 86201-086201. A. M. Elabsy, Influence of heat on impurity states in an artificial semiconductor atom. Egypt. J. Sol., Vol. (23), No. (2), (2000)
23. YP Varshni , Binding energy of a screened donor In a spherical quantum dot with parabolic Potential; superlattices and microstructures, *Vol29 (2001) pages 233-238*.
24. S Y L´opez1, N Porras-Montenegroand C A Duque, Binding energy and density of shallow impurities states in GaAs-(GaAl)As quantum wells: Effect of applied hydrostatic stress que1, Semicond. Sci. Technol. 18 (2003) 718–722
25. C. A. Duque, N. Porras-Montenegro, Z. Barticevic, M. Pacheco, and L. E. Oliveira, Effect of applied magnetic fields and hydrostatic pressure on the optical transition in self-assembled InAs /GaAs quantum dots. *J. Phys.:Condens. Matter* **18** (2006) 1877.
26. H Odhiambo Oyoko, Effect of uniaxial stress on the density of states of shallow donor impurities in GaAs quantum wells, Physica scripta Volume 66, p94-96, 2002
27. R. Khordad, Effect of position dependent effective mass of a hydrogenic donor impurity in a ridge quantum wire. Physica E volume 42,issue 5, (2010) p1503–1508
28. F.J. Ribeiro and a. Latge', Impurities in a quantum dots: A comparative study. Physical Review B volume 50, number 7 15 august 1994

APPENDIX

APPENDIX A: Detailed Calculation of Kinetic Energy

In this section, we have shown the initial development of the problem. The derivation of the expression which was used to calculate the total energy from a trial wave function in the effective mass approximation is shown. The approach is based upon the variational method in the effective mass approximation. We have used a trial wave function, which is a modified by an additional term that represents the hydrogenic impurity.

$$\psi(x,y,z) = N\cos\alpha x\cos\beta y\cos\lambda z e^{-\delta(x^2+y^2+z^2)^{\frac{1}{2}}}$$

Where δ is the variational parameter, $\alpha, \beta, and \lambda$ are constants and N represents the normalization constant. Therefore

$$\nabla^2\psi(x,y,z) = \left(\frac{\partial^2}{\partial x^2}+\frac{\partial^2}{\partial y^2}+\frac{\partial^2}{\partial z^2}\right) N\cos\alpha x\cos\beta y\cos\lambda z e^{-\delta(x^2+y^2+z^2)^{\frac{1}{2}}}$$

Differentiating the trial wave function with respect to x;

$$\nabla_x{}^2\psi(x,y,z) = \frac{\partial^2}{\partial x^2}\left[N\cos\alpha x\cos\beta y\cos\lambda z e^{-\delta(x^2+y^2+z^2)^{\frac{1}{2}}}\right]$$

This comes to

$$\nabla_x{}^2\psi(x,y,z) = N\cos(\beta y)\cos(\lambda z)\frac{\partial}{\partial x}\left\{\frac{\partial}{\partial x}\cos(\alpha x)e^{-\delta(x^2+y^2+z^2)^{\frac{1}{2}}}\right\}.$$

Then after simplification we get,

$$\nabla_x{}^2\psi(x,y,z) = N\cos(\beta y)\cos(\lambda z)\frac{\partial}{\partial x}\left\{-\alpha\sin(\alpha x)e^{-\delta(x^2+y^2+z^2)^{\frac{1}{2}}} + \frac{(-\delta x)e^{-\delta(x^2+y^2+z^2)^{\frac{1}{2}}}}{(x^2+y^2+z^2)^{\frac{1}{2}}}\cos(\alpha x)\right\}$$

This when differentiated a second time comes to;

$$\nabla_x{}^2\psi = N\cos(\beta y)\cos(\lambda z)\{-\alpha\left[\alpha\cos(\alpha x)e^{-\delta(x^2+y^2+z^2)^{\frac{1}{2}}} + (-\delta x)\sin(\alpha x)\frac{e^{-\delta(x^2+y^2+z^2)^{\frac{1}{2}}}}{(x^2+y^2+z^2)^{\frac{1}{2}}}\right]$$

$$+(-\delta y)\left[-\beta Sin(\beta y)\frac{e^{-\delta(x^2+y^2+z^2)^{\frac{1}{2}}}}{(x^2+y^2+z^2)^{\frac{1}{2}}} + (-\delta y)\frac{e^{-\delta(x^2+y^2+z^2)^{\frac{1}{2}}}}{(x^2+y^2+z^2)^{\frac{1}{2}}}\cos(\beta y) - y\frac{e^{-\delta(x^2+y^2+z^2)^{\frac{1}{2}}}}{(x^2+y^2+z^2)^{\frac{3}{2}}}\cos(\beta y)\right]\} \quad \text{(A1)}$$

Simplifying equation (A1) further yields;

$$\nabla_x{}^2(x,y,z) = N\cos(\beta y)\cos(\lambda z)\{-\alpha^2\cos(\alpha x)e^{-\delta(x^2+y^2+z^2)^{\frac{1}{2}}} + \alpha\delta x\sin(\alpha x)\frac{e^{-\delta(x^2+y^2+z^2)^{\frac{1}{2}}}}{(x^2+y^2+z^2)^{\frac{1}{2}}}$$

$$+\alpha\delta x\sin(\alpha x)\frac{e^{-\delta(x^2+y^2+z^2)^{\frac{1}{2}}}}{(x^2+y^2+z^2)^{\frac{1}{2}}} + \delta^2x^2\cos(\alpha x)\frac{e^{-\delta(x^2+y^2+z^2)^{\frac{1}{2}}}}{(x^2+y^2+z^2)} + \delta x^2\cos(\alpha x)\frac{e^{-\delta(x^2+y^2+z^2)^{\frac{1}{2}}}}{(x^2+y^2+z^2)^{\frac{3}{2}}}\} \quad \text{(A2)}$$

Collecting the like terms in equation (A2) and simplifying we get;

$$\nabla_x{}^2(x,y,z) = N\cos(\beta y)\cos(\lambda z)\{-\alpha^2\cos(\alpha x)e^{-\delta(x^2+y^2+z^2)^{\frac{1}{2}}} + 2\alpha\delta x\sin(\alpha x)\frac{e^{-\delta(x^2+y^2+z^2)^{\frac{1}{2}}}}{(x^2+y^2+z^2)^{\frac{1}{2}}}$$

$$+\delta^2x^2\cos(\alpha x)\frac{e^{-\delta(x^2+y^2+z^2)^{\frac{1}{2}}}}{(x^2+y^2+z^2)} + \delta x^2\cos(\alpha x)\frac{e^{-\delta(x^2+y^2+z^2)^{\frac{1}{2}}}}{(x^2+y^2+z^2)^{\frac{3}{2}}} \quad \text{(A3)}$$

Differentiating a second time with respect to y, we obtain,

$$\nabla_y{}^2\psi(x,y,z)=\frac{\partial^2}{\partial y^2}\left[N\cos\alpha x\cos\beta y\cos\lambda z e^{-\delta(x^2+y^2+z^2)^{\frac{1}{2}}}\right]$$

We break this down as;

$$\nabla_y{}^2\psi(x,y,z)=N\cos(\alpha x)\cos(\lambda z)\frac{\partial}{\partial y}\left\{\frac{\partial}{\partial y}\cos(\beta y)e^{-\delta(x^2+y^2+z^2)^{\frac{1}{2}}}\right\}$$

We differentiate the term in the bracket and get;

$$\nabla_y{}^2\psi(x,y,z)=N\cos(\alpha x)\cos(\lambda z)\frac{\partial}{\partial y}\left\{-\beta\sin(\beta y)e^{-\delta(x^2+y^2+z^2)^{\frac{1}{2}}}+\frac{(-\delta y)e^{-\delta(x^2+y^2+z^2)^{\frac{1}{2}}}}{(x^2+y^2+z^2)^{\frac{1}{2}}}\cos(\beta y)\right\} \quad \text{(A4)}$$

Differentiatingthe term in bracket in equation (A4) we obtain;

$$\nabla_y{}^2\psi(x,y,z)=N\cos(\alpha x)\cos(\lambda z)\{-\beta\left[\beta\cos(\beta y)e^{-\delta(x^2+y^2+z^2)^{\frac{1}{2}}}+(-\delta y)\sin(\beta y)\frac{e^{-\delta(x^2+y^2+z^2)^{\frac{1}{2}}}}{(x^2+y^2+z^2)^{\frac{1}{2}}}\right]$$

$$+(-\delta z)\left[-\beta Sin(\lambda z)\frac{e^{-\delta(x^2+y^2+z^2)^{\frac{1}{2}}}}{(x^2+y^2+z^2)^{\frac{1}{2}}}+(-\delta z)\frac{e^{-\delta(x^2+y^2+z^2)^{\frac{1}{2}}}}{(x^2+y^2+z^2)^{\frac{1}{2}}}\cos(\lambda z)-z\frac{e^{-\delta(x^2+y^2+z^2)^{\frac{1}{2}}}}{(x^2+y^2+z^2)^{\frac{3}{2}}}\cos(\lambda z)\right]\} \quad \text{(A5)}$$

Collecting like terms in equation (A5) and simplifying yields;

$$\nabla_y{}^2\psi(x,y,z)=N\cos(\alpha x)\cos(\lambda z)\{-\beta^2\cos(\beta y)e^{-\delta(x^2+y^2+z^2)^{\frac{1}{2}}}+2\beta\delta y\sin(\beta y)\frac{e^{-\delta(x^2+y^2+z^2)^{\frac{1}{2}}}}{(x^2+y^2+z^2)^{\frac{1}{2}}}$$

$$+\delta^2y^2\cos(\beta y)\frac{e^{-\delta(x^2+y^2+z^2)^{\frac{1}{2}}}}{(x^2+y^2+z^2)}+\delta y^2\cos(\beta y)\frac{e^{-\delta(x^2+y^2+z^2)^{\frac{1}{2}}}}{(x^2+y^2+z^2)^{\frac{3}{2}}}\} \quad \text{(A6)}$$

Lastly we repeat the differentiation with respect to z.

$$\nabla_z{}^2\psi(x,y,z)=\frac{\partial^2}{\partial z^2}\left[N\cos\alpha x\cos\beta y\cos\lambda z e^{-\delta(x^2+y^2+z^2)^{\frac{1}{2}}}\right]$$

We simplify as;

$$\nabla_z{}^2\psi(x,y,z)=N\cos(\alpha x)\cos(\beta y)\frac{\partial}{\partial z}\left\{\frac{\partial}{\partial z}\cos(\lambda z)e^{-\delta(x^2+y^2+z^2)^{\frac{1}{2}}}\right\}$$

Differentiating the term in the bracket again we get;

$$\nabla_z{}^2\psi=N\cos(\alpha x)\cos(\beta y)\frac{\partial}{\partial z}\left\{-\lambda\sin(\lambda z)e^{-\delta(x^2+y^2+z^2)^{\frac{1}{2}}}+\frac{(-\delta z)e^{-\delta(x^2+y^2+z^2)^{\frac{1}{2}}}}{(x^2+y^2+z^2)^{\frac{1}{2}}}\cos(\lambda z)\right\} \quad \text{(A7)}$$

Simplifying equation (A7) further, we get;

$$\nabla_z{}^2\psi=N\cos(\alpha x)\cos(\beta y)\left\{-\lambda\left[\lambda\cos\lambda z e^{-\delta\left[x^2+y^2+z^2\right]^{\frac{1}{2}}}+\left(-\delta z\right)\sin\lambda z\frac{e^{-\delta\left[x^2+y^2+z^2\right]^{\frac{1}{2}}}}{\left[x^2+y^2+z^2\right]^{\frac{1}{2}}}\right]\right.$$

$$\left.+(-\delta z)\left[-\beta Sin(\lambda z)\frac{e^{-\delta(x^2+y^2+z^2)^{\frac{1}{2}}}}{(x^2+y^2+z^2)^{\frac{1}{2}}}+(-\delta z)\frac{e^{-\delta(x^2+y^2+z^2)^{\frac{1}{2}}}}{(x^2+y^2+z^2)^{\frac{1}{2}}}\cos(\lambda z)-z\frac{e^{-\delta(x^2+y^2+z^2)^{\frac{1}{2}}}}{(x^2+y^2+z^2)^{\frac{3}{2}}}\cos(\lambda z)\right]\right\} \quad \text{(A8)}$$

Collecting like terms in equation (A8) we get;

$$\nabla_z{}^2(x,y,z)=N\cos(\alpha x)\cos(\beta y)\{-\lambda^2\cos(\lambda z)e^{-\delta(x^2+y^2+z^2)^{\frac{1}{2}}}+\lambda\delta z\sin(\lambda z)\frac{e^{-\delta(x^2+y^2+z^2)^{\frac{1}{2}}}}{(x^2+y^2+z^2)^{\frac{1}{2}}}$$

$$+\delta^2\lambda^2\cos(\lambda z)\frac{e^{-\delta(x^2+y^2+z^2)^{\frac{1}{2}}}}{(x^2+y^2+z^2)}+\delta z^2\cos(\lambda z)\frac{e^{-\delta(x^2+y^2+z^2)^{\frac{1}{2}}}}{(x^2+y^2+z^2)^{\frac{3}{2}}} \quad \text{(A9)}$$

Simplifying equation (A9) further yields;

$$\nabla_z{}^2\psi 9x,y,z) = N\cos(\alpha x)\cos(\beta y)\{-\lambda^2\cos(\lambda z)e^{-\delta(x^2+y^2+z^2)^{\frac{1}{2}}} + 2\lambda\delta z\sin(\lambda z)\frac{e^{-\delta(x^2+y^2+z^2)^{\frac{1}{2}}}}{(x^2+y^2+z^2)^{\frac{1}{2}}}$$

$$+\delta^2 z^2\cos(\lambda z)\frac{e^{-\delta(x^2+y^2+z^2)^{\frac{1}{2}}}}{(x^2+y^2+z^2)} + \delta z^2\cos(\lambda z)\frac{e^{-\delta(x^2+y^2+z^2)^{\frac{1}{2}}}}{(x^2+y^2+z^2)^{\frac{3}{2}}}\} \qquad \text{(A10)}$$

Combining equations (A3), (A6) and (A10) gives us;

$$\nabla^2\psi(x,y,z) = Ne^{-\delta(x^2+y^2+z^2)^{\frac{1}{2}}}\cos\alpha x\cos\beta y\cos\lambda z\left\{-\left(\alpha^2+\beta^2+\lambda^2-\delta^2-\frac{2\delta}{\left[x^2+y^2+z^2\right]^{\frac{1}{2}}}\right)\right\}$$

$$+\frac{2N\alpha\delta x\sin\alpha x\cos\beta y\cos\lambda z}{[x^2+y^2+z^2]^{\frac{1}{2}}}e^{-\delta(x^2+y^2+z^2)^{\frac{1}{2}}} + \frac{2N\beta\delta y\cos\alpha x\sin\beta y\cos\lambda z}{[x^2+y^2+z^2]^{\frac{1}{2}}}e^{-\delta(x^2+y^2+z^2)^{\frac{1}{2}}} + \frac{2N\lambda\delta z\cos\alpha x\cos\beta y\sin\lambda z}{[x^2+y^2+z^2]^{\frac{1}{2}}}e^{-\delta(x^2+y^2+z^2)^{\frac{1}{2}}} \qquad \text{(A10)}$$

Using equation (A10), the kinetic energy T is given as;

$$\langle T\rangle = -\frac{\hbar^2}{2m}\{-(\alpha^2+\beta^2+\lambda^2-\delta^2)\frac{\int_0^{\frac{L_x}{2}}\cos^2\alpha x dx\int_0^{\frac{L_y}{2}}\cos^2\beta y dy\int_0^{\frac{Lz}{2}}\cos^2\lambda z dz}{\int_0^{\frac{L_x}{2}}\cos^2\alpha x dx\int_0^{\frac{L_y}{2}}\cos^2\beta y dy\int_0^{\frac{Lz}{2}}\cos^2\lambda z dz}$$

$$-2\delta\frac{\int_0^{\frac{L_x}{2}}\cos^2\alpha x dx\int_0^{\frac{L_y}{2}}\cos^2\beta y dy\int_0^{\frac{L_z}{2}}\frac{\cos^2\lambda z(e^{-2\delta(x^2+y^2+z^2)^{\frac{1}{2}}})}{(x^2+y^2+z^2)^{\frac{1}{2}}}dz}{\int_0^{\frac{L_x}{2}}\cos^2\alpha x dx\int_0^{\frac{L_y}{2}}\cos^2\beta y dy\int_0^{\frac{L_z}{2}}\cos^2\lambda z dz}$$

$$+\frac{\alpha\delta\int_0^{\frac{L_x}{2}}x\sin(2\alpha x)dx\int_0^{\frac{L_y}{2}}Cos^2(\beta y)dy\int_0^{\frac{L_z}{2}}\cos^2(\lambda z)\frac{e^{-2\delta(x^2+y^2+z^2)^{\frac{1}{2}}}}{(x^2+y^2+z^2)^{\frac{1}{2}}}dz}{\int_0^{\frac{L_x}{2}}\cos^2\alpha x dx\int_0^{\frac{L_y}{2}}\cos^2\beta y dy\int_0^{\frac{L_z}{2}}\cos^2\lambda z dz}$$

$$+\frac{\beta\delta\int_0^{\frac{L_x}{2}} Cos^2(\alpha x)dx\int_0^{\frac{L_y}{2}} ySin(2\beta y)dy\int_0^{\frac{L_z}{2}} \cos^2(\lambda z)\dfrac{e^{-2\delta(x^2+y^2+z^2)^{\frac{1}{2}}}}{(x^2+y^2+z^2)^{\frac{1}{2}}}dz}{\int_0^{\frac{L_x}{2}} \cos^2\alpha x dx\int_0^{\frac{L_y}{2}} \cos^2\beta y dy\int_0^{\frac{L_z}{2}} \cos^2\lambda z dz}$$

$$+\frac{\lambda\delta\int_0^{\frac{L_x}{2}} Cos^2(\alpha x)dx\int_0^{\frac{L_y}{2}} Cos^2(\beta y)dy\int_0^{\frac{L_z}{2}} zSin(2\lambda z)\dfrac{e^{-2\delta(x^2+y^2+z^2)^{\frac{1}{2}}}}{(x^2+y^2+z^2)^{\frac{1}{2}}}dz}{\int_0^{\frac{L_x}{2}} \cos^2\alpha x dx\int_0^{\frac{L_y}{2}} \cos^2\beta y dy\int_0^{\frac{L_z}{2}} \cos^2\lambda z dz}\} \quad \text{A11)}$$

Where the double angle trigonometric identity $\sin 2\alpha x = 2\sin\alpha x\cos\alpha x$

Has been applied for $\sin 2\beta y$ and $\sin 2\lambda z$ to simplify equation (A11).

Taking the ground state where n=1 we have $\alpha = \frac{\pi}{L_x}, \beta = \frac{\pi}{L_y}, \lambda = \frac{\pi}{L_z}$

APPENDIX B: Detailed Calculation of Free Energy

The free energy E_{free} is given by;

$$E_{free} = \frac{\langle \psi_{free} | H_{free} | \psi_{free} \rangle}{\langle \psi_{free} | \psi_{free} \rangle} \tag{B1}$$

Where H is the Hamiltonian for the free particle and is given by;

$$H_{free} = -\frac{\hbar^2}{2m^*}\left\{\frac{\partial^2}{\partial x^2} + \frac{\partial^2}{\partial y^2} + \frac{\partial^2}{\partial z^2}\right\}$$

ψ_{free}, is the free particle ground state wave function given by,

$$\psi_{free}(x, y, z) = N \cos \alpha x \cos \beta y \cos \lambda z$$

We then differentiate ψ_{free} with respect to *x*, twice as;

$$\nabla_x{}^2 \psi_{free}(x, y, z) = \frac{\partial}{\partial x}\left\{\frac{\partial}{\partial x}\left(N \cos \alpha x \cos \beta y \cos \lambda z\right)\right\}$$

This simplifies to,

$$= \frac{\partial}{\partial x}\{-\alpha Sin\alpha x Cos\beta y Cos\lambda z\}$$

Finally yielding;

$$\nabla_x{}^2 \psi_{free}(x, y, z) = \alpha^2 N \cos \alpha x \cos \beta y \cos \lambda z \tag{B2}$$

We do the same for the y-component of ψ_{free},

$$\nabla_y{}^2\psi(x,y,z)=\frac{\partial}{\partial y}\left\{\frac{\partial}{\partial y}\left(N\cos\alpha x\cos\beta y\cos\lambda z\right)\right\}$$

We simplified as,

$$\nabla_y{}^2\psi(x,y,z)=\frac{\partial}{\partial y}\left\{-N\beta\cos\alpha x\sin\beta y\cos\lambda z\right\}$$

Differentiating a second time we obtain,

$$\nabla_y{}^2\psi(x,y,z)=\beta^2 N\cos\alpha x\cos\beta y\cos\lambda z \qquad \text{(B3)}$$

We also do the differentiation with respect to z,

$$\nabla_z{}^2\psi_{free}(x,y,z)=\frac{\partial}{\partial z}\left\{\frac{\partial}{\partial z}\left(N\cos\alpha x\cos\beta y\cos\lambda z\right)\right\}$$

This gives;

$$\nabla_z{}^2\psi_{free}(x,y,z)=\frac{\partial}{\partial z}\left\{-N\lambda\cos\alpha x\cos\beta y\sin\lambda z\right\}$$

On differentiating a second time we get;

$$\nabla_z{}^2\psi_{free}(x,y,z)=\lambda^2 N\cos\alpha x\cos\beta y\cos\lambda z \qquad \text{(B4)}$$

We do the substitutions in equation (B2), (B3) and (B4) in equation (B1);

$$=\frac{-\hbar^2}{2m^*}\left\{\frac{\alpha^2\int\cos^2\alpha x\cos^2\beta y\cos^2\lambda z d\tau+\beta^2\int\cos^2\alpha x\cos^2\beta y\cos^2\lambda z d\tau+\lambda^2\int\cos^2\alpha x\cos^2\beta y\cos^2\lambda z d\tau}{\int\cos^2\alpha x\cos^2\beta y\cos^2\lambda z d\tau}\right\}$$

(B5)

Finally simplifying equation (B5) further we obtain the free energy equation;

$$\nabla^2\psi(x,y,z) = \frac{-\hbar^2}{2m}\left(\alpha^2 + \beta^2 + \lambda^2\right)$$

Where m^* the effective mass of an electron and *h* is Planck's constant and $\alpha = \frac{2.4048}{a_0}$.

Where a_0 is the Bohr radius.

APPENDIX C: Python Code for Computation of Binding Energy and Density of Impurity States

```
fromnumpy import *
fromscipy.integrate import quad,dblquad,tplquad
importmatplotlib.pyplot as plt
fromscipy import sparse
fromscipy import optimize
fromscipy import special
import sys, time, os, shutil
start_time = time.time()
#Methods for Integrating Functions
#odeint                    #Integrate ordinary differential equations.
#quad                      #General purpose integration.
#dblquad                    #General purpose double integration.
#tplquad                    #General purpose triple integration.
#declare constants
e=1
pi=3.14159
epsilon0=12.56
hbar=1
mstar=0.067

print
print ('Processing..')

fori in range(20):
sys.stdout.write(".")
```

```
sys.stdout.flush()

time.sleep(.2)

print

print ('Your results are written in the file named: length_to_plot.txt')

print

outfile = open("data_E_de.txt", 'w')

outfile.write("#Length, delta,  Energy \n")

outfile.close()

L=100

for L in arange(2.74,9.0,0.1):

outfile = open("data_E_de.txt", 'a')

alpha=   pi/L

beta=    pi/L

lambdah= pi/L

#delta is a variable parameter. make a loop

delta=0.1

#integration function 1

 func1= lambda x,y,z :  cos(alpha*x)**2 * cos(beta*y)**2 * cos(lambdah*z)**2*exp(-
                    2*delta* sqrt(x**2 + y**2 + z**2))

x0,x1= 0, L/2.

 y0,y1= lambda y: 0, lambda y:  L/2.

 z0,z1= lambda x,y: 0, lambda x,y:  L/2.

 res1, err = tplquad(func1, x0,x1,y0,y1,z0,z1)

rho1 = 0.

 rho2 = 2.4

# limits for theta

 theta1 = 0

 theta2 = 2*pi
```

```
# limits for phi

 phi1 = 0

 phi2 = pi

delta=0.1

 #integration function 2

 func2= lambda x,y,z :  cos(alpha*x)**2 * cos(beta*y)**2 * cos(lambdah*z)**2*exp(-
                2*delta* sqrt(x**2 + y**2 + z**2))/sqrt(x**2 + y**2 + z**2)

x0,x1= 0, L/2.

 y0,y1= lambda y: 0, lambda y:  L/2.

 z0,z1= lambda x,y: 0, lambda x,y:  L/2.

 res2, err2 = tplquad(func2, x0,x1,y0,y1,z0,z1)

#integration function 3

 func3= lambda x,y,z :  cos(alpha*x)**2 * cos(beta*y)**2 * y*sin(2*beta*z)**2*exp(-
                2*delta* sqrt(x**2 + y**2 + z**2))/sqrt(x**2 + y**2 + z**2)

x0,x1= 0, L/2.

 y0,y1= lambda y: 0, lambda y:  L/2.

 z0,z1= lambda x,y: 0, lambda x,y:  L/2.

 res3, err3 = tplquad(func2, x0,x1,y0,y1,z0,z1)

def E(min_delta):

  return      (hbar**2/(2*mstar))* (-(alpha**2 +beta**2+lambdah**2-min_delta**2)- (-
                2*min_delta * res2/res1) - (alpha*min_delta*res3*3/res1)) +
                e**2/12.56*(-(alpha**2 +beta**2+lambdah**2-min_delta**2)+ (-
                2*min_delta * res2/res1) + (alpha*min_delta*res3*3/res1))/27211

min_delta=optimize.brent(E)

min_E=      (hbar**2/(2*mstar))* (-(alpha**2 +beta**2+lambdah**2-min_delta**2)+ (-
                2*min_delta * res2/res1) + (alpha*min_delta*res3*3/res1)) -
                e**2/12.56*(-(alpha**2 +beta**2+lambdah**2-min_delta**2)+ (-
                2*min_delta * res2/res1) + (alpha*min_delta*res3*3/res1))/27211

alphah=2.4048

Ebh= ((hbar**2)*(alphah**2)/(2*mstar)) - min_E

 #Enh=(hbar**2/(2*mstar))*  (-(alpha**2 +beta**2+lambdah**2-min_delta**2)+ (-
                2*min_delta                 *                 res2/res1)                 +
```

```
                (alpha*min_delta*res3*3/res1))+(e**2/12.56**2)*(13.56-(exp(-
                L**(15/8))))*(-(alpha**2 +beta**2+lambdah**2-min_delta**2)+ (-
                2*delta * res2/res1) + (alpha*min_delta*res3*3/res1))

 #Ebnh= ((hbar**2*alphah**2)/(2*mstar)) - Enh

funcEb= lambda l : l/Ebh

re, er = quad(funcEb, 0,L/2)

gEb=(L/Ebh*pi)*re

print(L*5.2917, min_delta/5.2917, min_E,Ebh,gEb)

outfile.write("%-9s %-9s %s %s %s \n" % (L*5.2917, min_delta*5.2917,
                min_E,Ebh,gEb))

outfile.close()

data =loadtxt('data_E_de.txt') # read the file

x1 = data[:,4]  #delta

y1 = data[:,3]

plt.plot(x1,y1)

xmin=min(x1)

xmax=max(x1)

ymin=min(y1)

ymax=max(y1)

plt.xlabel('bINDINGeNERGY(MeV)')

plt.ylabel("Density of impurity state (nm^-^1)")

plt.savefig('Binding energy(meV)')

plt.show()
```

APPENDIX D: Tables of Results

Table 1: Binding energy as a function of quantum well dot size for the hydrogenic donor

Quantum Dot size (nm)	Binding Energy (meV)
15.557598	51.220149335
16.086768	53.406517889
16.615938	54.935745266
17.145108	55.963844476
17.674278	56.097601616
18.203448	56.964600083
18.732618	57.098434001
19.261788	57.065327838
19.790958	56.907116335
20.320128	56.562338384
20.849298	56.337857999
21.378468	55.971544003
21.907638	55.572472644
22.436808	55.152411919

22.965978	54.720459755
23.495148	54.283620133
24.024318	53.847252338
24.553488	53.415421855
25.082658	52.991176133
25.611828	52.576760999
26.140998	52.173791711
26.670168	51.783388188
27.199338	51.406282033
27.728508	51.042901511
28.257678	50.693439093
28.786848	50.357905075
29.316018	50.036170293
29.845188	49.728000133
30.374358	49.433081366
30.903528	49.151043933
31.432698	48.881477477

31.961868	48.623945 1
32.491038	48.377993 86
33.020208	48.143162 85
33.549378	47.918989 999
34.078548	47.705016 68
34.607718	47.500791 86
35.136888	47.305874 5
35.666058	47.119836 04
36.195228	46.942261 61
36.724398	46.772751 32
37.253568	46.610920 38
37.782738	46.456400 05
38.311908	46.308837 22
38.841078	46.167894 85
39.370248	46.033250 79
39.899418	45.904598 44
40.428588	45.781646 05

40.957758	45.664115757
41.486928	45.551743777
42.016098	45.444279299
42.545268	45.341484432
43.074438	45.243132929
43.603608	45.149010577
44.132778	45.058914061
44.661948	44.972650173
45.191118	44.890036258
45.720288	44.810898577

Table 2: The binding energy as a function of quantum well dot size for the non-hydrogenic donor

Quantum Dot size (nm)	Binding Energy (meV)
15.557598	51.313019
16.086768	53.524573
16.615938	55.071415
17.145108	56.111358
17.674278	56.764714
18.203448	57.123642
18.732618	57.259017
19.261788	57.225530
19.790958	57.065496
20.320128	56.811724
20.849298	56.489681
21.378468	56.119147
21.907638	55.715479
22.436808	55.290580
22.965978	54.853652
23.495148	54.411781
24.024318	53.970387
24.553488	53.533582
25.082658	53.104450
25.611828	52.685261
26.140998	52.276504
26.670168	51.882750
27.199338	51.501300
27.728508	51.133734

28.257678	50.780246262
28.786848	50.440847352
29.316018	50.115406633
29.845188	49.803686788
30.374358	49.505370960
30.903528	49.220084840
31.432698	48.947413361
31.961868	48.686914578
32.491038	48.438130318
33.020208	48.200594378
33.549378	47.973839368
34.078548	47.757401378
34.607718	47.550824168
35.136888	47.353616262
35.666058	47.165480268
36.195228	46.985860428
36.724398	46.814396768
37.253568	46.650702598
37.782738	46.494402418
38.311908	46.345139868
38.841078	46.202574038
39.370248	46.066379068

39.899418	45.936244818
40.428588	45.811876188
40.957758	45.692992099
41.486928	45.579325748
42.016098	45.470623428
42.545268	45.366644396
43.074438	45.267160118
43.603608	45.171953611
44.132778	45.080819319
44.661948	44.993561796
45.191118	44.909993627
45.720288	44.829947038

Table 3: Variation of Binding energy with Density of Impurity states for Hydrogenic donor impurity

Binging Energy(meV)	Density of Impurity states(/nm)
9.8373885260754309	0.89218549740447661
9.8383885260754323	0.91158649934600144
9.8453885260754339	0.97373807027561488
9.8553885260794339	1.0704831793113359
9.8761305664699588	1.1014196973532457
10.003446755406836	1.122218666370197
10.194533188265707	1.1352862124665415
10.434354306114914	1.1424653403062159
10.71251048509774	1.1451734850482367
11.02151412076276	1.1445044061927683
11.355786470232573	1.1413043823503948
11.711046870756014	1.1362295499868491
12.083926810952281	1.1297892663819218
12.471717728539781	1.1223791219784238
12.872201080295545	1.1143062326919906
13.283531257950958	1.1058086698219138
13.704152641620656	1.0970704911712845
14.132739786604173	1.0882333943819043
14.568153239255423	1.0794058019853605
15.009406276407795	1.0706699666100905

15.455639462034856	1.0620875409662085
15.906100761252473	1.0537039629222849
16.360129772137324	1.0455519136848488
16.817145004051909	1.037654052485161
17.276633476717763	1.0300251822521751
17.738142059262547	1.0226739698272089
18.201270213459587	1.0156043112247228
18.665663840498997	1.008816416457069
19.131009976753077	1.0023076737811472
19.59703216592602	0.99607333891626126
20.063486534284863	0.9901070771547229
20.530158209624606	0.98440140067062631
20.996858238570766	0.97894801119832631
21.463420867435815	0.97373807027561488
21.929701046505759	0.96876241549709685
22.395572383281156	0.9640117219971035
22.860924932072248	0.95947664437554081
23.325663742733632	0.95514790410278438
23.789707050934549	0.95101637661969873
24.252985072476278	0.94707314029815226

24.715438608156379	0.94330952404528756
25.177017840276228	0.939717139548226
25.637681584376466	0.93628789092253117
26.097396022422394	0.93301400044592031
27.013874955504495	0.92690275877020611
27.470602436114866	0.92405144608663048
27.92630563602517	0.9213275502537398
28.38097744415467	0.91872487143978898
28.834614563373016	0.91623750217109778
27.013874955504495	0.92690275877020611
29.287216926359335	0.91385982281267786
29.738787039542391	0.91158649934600144
30.189330196677709	0.90941245455631914
30.638853556297946	0.90733287588230227
31.087366254085467	0.90534319177598621
31.534879062651754	0.90343906329358514
31.981403973069479	0.90161637856348464
32.426954436117789	0.89987122913817441
32.871544507827551	0.89819991869729476
33.315189307721788	0.89659893515967626

33.757904601480483	0.89506494868892827
34.199706725413719	0.89359480079036147
34.640612391985613	0.89218549740447661

Table 4: Variation of Binding energy with Density of Impurity states for Non-Hydrogenic donor Impurity

Binging Energy(meV)	Density of Impurity states(/nm)
13.632853362412287	0.9108049620063382 13
13.633067241042678	0.9998921864985849 1
13.635943906496823	1.0649110792987055
13.638755797041518	1.1116351012963861
13.651888363214066	1.1444177250006 12
13.746548383844926	1.1665615424555942
13.868123161243446	1.1805853730046705
14.014173510984211	1.1884192399480511
14.183471535738928	1.1915480934399063
14.375501253278047	1.1911182914431517
14.590181650164149	1.1880172387984957
14.827704594482963	1.1829333291891351
15.088435856464111	1.1764012849186269
15.372852361751542	1.1688366809565536
15.681501067100715	1.1605624016195646

16.014971590705908	1.151828968914214 5
16.373877517389197	1.142830272909700 9
16.758843643400724	1.133715769857178 3
17.170497175403028	1.124599994626598 5
17.609461701125657	1.115570002523280 4
18.076353184528074	1.106691204583724 7
18.571773586433888	1.098011963356167 1
19.096328169623742	1.089567218294385 2
19.650586970383941	1.081381353935501 7
20.235122277401274	1.073470472229836 3
20.850489900111231	1.065844198146641 8
21.497233372665008	1.058507113596987 7
22.175884598580716	1.051459897440659 7
22.886964603827995	1.044700234160093 5
23.630984328114778	1.038223538941244 9
24.408445586857344	1.032023528722036 7
25.219841886562964	1.026092682883116 7
26.065659322052159	1.020422604818183 7

26.946377469523767	1.015004307413607
27.862470138678788	1.009828441645431 3
28.814406338285599	1.004885467895190 6
29.802650631900203	1.000016580605383 0 1
31.889905303101582	0.991358455640101 5
32.989829764770192	0.987252202550103 7 1
34.127891692336362	0.983332236170368 4 7
35.304543615320398	0.979589907032135 5 5
36.520237440758017	0.976016861280793 0 1
37.775424209113211	0.972605068228674 1
39.070554986624238	0.969346816423850 5 7
40.406080793946887	0.966234723723006 5 6
41.782452700179405	0.963261738093345 2 5
43.200122891286185	0.960421119217894 7 5
44.659543727801143	0.957706450743813 4 4
46.161168845261258	0.955111616803644 5 4
47.705453002264399	0.952630797646631 3 9
9.292851555717192 4	0.950258467581088 0 1

50.923821934348823	0.947989365571373 7
52.598822239813487	0.945818503429114 89
54.318312290219986	0.943741141643061 55
56.082753477073304	0.941752780816412 23
57.892608272300457	0.939849156043234 05
59.748341504966675	0.938026212644969 33
61.650418462588092	0.936280115146083 78
63.599306672521209	0.934607218620903 68
65.595475131197077	0.933004066648282 06
67.639394459225301	0.931467380099286 65
69.731536632502383	0.929940500287761 1